Scanning tunneling microscopy study of morphology and electronic properties in (K0.7Na0.3)Fe2−ySe2 single crystal

A. S. Trifonov, Y. A. Ovchenkov, D. E. Presnov, R. Belosludov, A. I. Boltalin, M. Liu, I. V. Morozov, H. Nejo, and A. N. Vasiliev

Articles you may be interested in

Giant increase of critical current density and vortex pinning in Mn doped KxFe2−ySe2 single crystals
Appl. Phys. Lett. **105**, 192602 (2014); 10.1063/1.4901902

Anisotropic transport property anomaly in K0.8Fe1.65Se2 crystal
J. Appl. Phys. **115**, 143905 (2014); 10.1063/1.4871456

Evidence for multiple nodeless gaps and electron-mode coupling from scanning tunneling spectroscopy in the iron-based superconductor Ba0.6K0.4Fe2As2
AIP Conf. Proc. **1447**, 12 (2012); 10.1063/1.4709862

Giant magnetic flux jumps in single crystals of Ba 0.6 K 0.4 Fe 2 As 2
Appl. Phys. Lett. **98**, 182505 (2011); 10.1063/1.3586777

Electronic structures of two-phase microstructures α and β in heavily Pb-doped Bi 2 Sr 2 CaCu 2 O y single crystals investigated by scanning tunneling microscopy/spectroscopy
Appl. Phys. Lett. **83**, 1178 (2003); 10.1063/1.1594826

CrossMark
← click for updates

Scanning tunneling microscopy study of morphology and electronic properties in $(K_{0.7}Na_{0.3})Fe_{2-y}Se_2$ single crystal

A. S. Trifonov,[1,2,a)] Y. A. Ovchenkov,[2] D. E. Presnov,[1,2] R. Belosludov,[3] A. I. Boltalin,[4] M. Liu,[4] I. V. Morozov,[4] H. Nejo,[5] and A. N. Vasiliev[2,6,7]

[1]*Skobeltsyn Institute of Nuclear Physics, Lomonosov Moscow State University, 1(2), Leninskie Gory, GSP-1, Moscow 119991, Russia*
[2]*Low Temperature Physics and Superconductivity Department, Physics Faculty, Lomonosov Moscow State University, 119991 Moscow, Russia*
[3]*Institute for Materials Research, Tohoku University, 980-8577 Sendai, Japan*
[4]*Department of Chemistry, Lomonosov Moscow State University, 119991 Moscow, Russia*
[5]*National Institute for Material Science, Tsukuba 305-0047, Japan*
[6]*Theoretical Physics and Applied Mathematics Department, Institute of Physics and Technology, Ural Federal University, Ekaterinburg 620002, Russia*
[7]*National University of Science and Technology "MISiS," Moscow 119049, Russia*

We investigated the microstructure of the iron selenide superconductor $(K_{0.7}Na_{0.3})Fe_{2-y}Se_2$ with a $T_c = 32$ K and a near 100% Meissner screening volume fraction. Topography and electron transport properties were studied using electron microscopy and ultra-high vacuum scanning tunneling microscopy (STM) techniques. Room temperature STM measurements reliably identify spatial variations of the local electronic properties of this material. The studied crystals consist of continuous regions with significantly different shapes of current-voltage curves reflecting different electronic transport properties of these regions. Fitting of the local current-voltage curves with the Simmons model for metal-dielectric-metal structure confirmed a phase separation in the sample to a metal and semiconducting phases. The observed regions have dimensions in the range of several tenths of a micrometer and indicate a phase separation in the sample. © *2014 AIP Publishing LLC*. [http://dx.doi.org/10.1063/1.4891227]

I. INTRODUCTION

The importance of a material microstructure along with the used preparative techniques (sputtering, quenching, etc.) for the thermodynamic properties of prepared superconductors, such as a T_c, was first realized during the study of the superconducting A15 alloys.[1] The optimal conditions for superconductivity are often near the border of a structural stability that makes the material prone to a phase separation. For example, a phase separation is a common phenomenon for a cuprate high temperature superconductor (HTS). It could be a property of certain samples but a phase separation can claim to be the most simple explanation for many common peculiarities of HTS: a coexistence of magnetic order and superconductivity, a positive curvature region on $H_c(T)$ curve, multi-gap and even a pseudo-gap phenomena. Indeed, a phase separation and proximity effect makes the system similar to one with strong time fluctuations which are usually used to explain a pseudo-gap.

As a continuation of the general trend, a phase separation is often observed in Fe based superconductors. For example, in a recent paper on the superconductivity in Pr doped $CaFe_2As_2$,[2] it was observed that the superconductivity emerges from clover like defects associated with Pr dopants. The authors call attention to the fact that all HTS are doped

systems and dopants are potential sources of inhomogeneity such as a phase separation, crystalline, or electronic disorder.

As a rule, a superconductivity of iron compounds occurs in non-stoichiometric compositions and a phase separation can be consequence of the structure defects ordering. In iron superconductors with the simplest structure, such as FeTe and FeSe, the iron content can vary to a fairly large extent. This leads to a formation of different crystalline and magnetic structures at low temperatures.[3,4] In particular, the variation of excess Fe leads to a competing coexistence of orthorhombic and monoclinic phases in FeTe at low temperatures.[5] The $Fe_{1+x}(Te_{1-y}Se_y)$ series can show a coexistence of superconductivity and magnetism in a wide range of y, possibly due to a perceptible phase separation at some x.[6–8]

For intercalated compounds, the picture becomes more complicated since a possible non-stoichiometry of another element is added. Among intercalated compounds, the Fe-based chalcogenides $AFe_{2-y}Se_2$ ($A =$ K, Rb, Cs, K/Tl, and Rb/Tl)[9] are of special interest. These were proposed to be heavily electron overdoped systems. Band structure calculations[10] predicted that in stoichiometric compounds the hole pockets which are found in other iron superconductors might be missing. In fact, intercalated iron chalcogenides do demonstrate unusual transport properties. The temperature dependence of resistivity shows a transition from a metallic behavior at low temperatures to a semiconducting behavior at higher temperatures. But, even at low temperature, near the superconducting transition point, the sample resistivity is usually in the range from a tenth to hundreds mΩ cm. This is

a)Author to whom correspondence should be addressed. Electronic mail: trifonov.artem@phys.msu.ru

nearly two order higher than corresponding values for the closest analogues—the 122 Fe arsenide family, and definitely violates the Ioffe-Regel criteria[11] for a metal resistivity which corresponds to the limit when an electron mean free path is equal to an interatomic distance.

Muon-spin rotation (MSR) measurements indicated a microscopic coexistence between the metallic superconducting phase and a strong magnetic phase which is semiconducting.[12–14] The semiconducting nature of the antiferromagnetic phase is one of the key features of intercalated iron chalcogenides.

A thorough study of superconducting $K_xFe_{2-y}Se_2$ samples by high-resolution synchrotron diffraction revealed a coexistence of separate metallic ($K_xFe_2Se_2$) and semiconducting ($K_2Fe_4Se_5$) phases. This allowed a fit of $R(T)$ to the full temperature range using a model of two, metallic and semiconducting, percolating phases.[15] The parallel conductivity of both phases describes well the shape of $R(T)$ and explains the wide variation in the position of the maximum on the $R(T)$ curves. On the other hand, if phases are separate and independent then the position of the maximum on the $R(T)$ curve should correlate with the absolute value of the resistivity. The higher content of a semiconducting phase, the higher resistivity and the lower temperature of the $R(T)$ maximum. But such behavior is not observed. Two possible explanations are a different "quality" of semiconducting/insulating phase or a complicated microstructure of samples. The MSR investigation showed that the volume of the insulating phase is near 88% while the sample shows a resistive superconducting transition.[14] Moreover, despite the low volume of a superconducting phase the samples can show a full Meissner screening. The last facts can reflect a complicated microstructure of the investigated samples.

In support of this speculation, some authors have reported an unusual sample structure in iron superconductors as, for example, a nanoscale inhomogeneity in these materials.[16,17] These structural features could explain both the bulk superconductivity and the full Meissner screening effect even at an extremely low specific fraction of a superconducting phase.

It is worth noting that the early investigations of cuprate HTS samples often revealed a grain boundary superconductivity and other structural peculiarities.[18] More recent works have not confirmed exclusive importance of such microstructural features. Nevertheless, the study of cuprate HTS microstructure is still continuing and the study of microstructural features of an iron HTS seems to be an important task. For an iron HTS, the 122 Fe chalcogenide phase is a convenient object for studying its microstructure using microprobe techniques such as a scanning tunneling microscopy (STM) because of a large difference between constituting phases electronic properties. STM allows one to investigate the local electronic transport properties of the sample. It has already been used to study an iron HTS at low temperatures.[19–21] In particular, STM low temperature spectroscopy has yielded useful information on local superconducting properties and allowed one to observe a phase separation between superconducting and non-superconducting phases.

In this study, we experimentally investigated the morphology of $(K_{0.7}Na_{0.3})Fe_{2-y}Se_2$ crystals using SEM, AFM, and STM techniques. The selected composition has $T_c = 32$ K and a near 100% Meissner screening volume fraction that are some of the best values for 122 iron chalcogenides. Our goal was to study the probable phase separation in high quality $(K_{0.7}Na_{0.3})Fe_{2-y}Se_2$ single crystal by studying the local electronic properties with STM at room temperatures similar to the method used previously for studying metallic and insulating phases in other compounds, for example, in manganites.[22] The room temperature was selected to ensure a sufficient conductivity of the expected semiconducting phase for a STM experiment. The important issue was to (check) determine the characteristic size of phase domains formed by a phase separation.

II. SAMPLES

The $(K_{0.7}Na_{0.3})Fe_{2-y}Se_2$ single crystals were grown by self-flux method, as described in detail elsewhere.[23] Crystals with dimensions up to $15 \times 10 \times 0.5$ mm^3 were obtained after $Na_{0.8}(Fe_{1.02}Se)_2$ and $K_{0.8}(Fe_{1.02}Se)_2$ precursors were heated up to $1030\,°C$ and kept for 2 h then slowly cooled down to $700\,°C$ and quenched in water. Results of XRD and energy dispersive X-ray (EDX) investigations, heat capacity measurements, magnetic and transport properties measurements along with other data are reported in Ref. 23. In brief, the EDX analysis yields the composition of the crystal to be $(Na_{0.32(2)}K_{0.68(2)})_{0.95(4)}Fe_{1.75(2)}Se_2$. The distribution curves of all elements do not show any features associated with microscopic inhomogeneities in the element distribution.

X-ray powder diffraction resolved the majority phase $(K,Na)_2Fe_4Se_5$, which can be indexed in the well-known supercell of the original $ThCr_2Si_2$ subcell with the space group I4/mmm. The second phase described by the space group I4/mmm could be a variant of vacancy disordered structure whose composition corresponds to the superconducting phase, and according to Ref. 15 may be described as a $(K,Na)_xFe_2Se_2$.

The refinement of unit cells parameters showed that sodium doping moderately decreased the parameter a of the main phase whereas the parameter c remained almost the same.[23] Transport property including the data on $H_{c2}(T)$ were generally very similar to those reported for other intercalated selenides as, for example, $K_xFe_{2-y}Se_2$ and $Rb_xFe_{2-y}Se_2$.[24] The onset of the superconducting transition at near 33 K and zero resistivity at 31.7 K are one of the highest reported for intercalated chalcogenides.

Fig. 1 shows the temperature dependence of resistivity for our sample. Insets show resistivity and magnetic susceptibility at low temperature, near the superconducting transition point. The absolute values of resistivity at low temperatures are in tenth mΩ cm range, which may correspond to a high content of a "non-superconducting" semiconducting phase. While the main phase is supposed to be a non-superconducting ($K_2Fe_4Se_5$), AC susceptibility measurements determine the value of diamagnetic screening at low temperatures as high as 96%. The heat capacity data confirm this value for the volume fraction of the superconducting phase.

III. RESULTS AND DISCUSSIONS

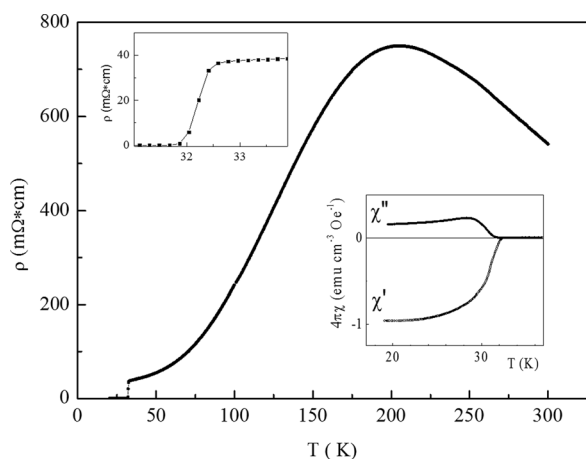Since our experience testified to moderate stability of the studied materials at atmosphere conditions, we did some

FIG. 1. Temperature dependence of resistivity for $(K_{0.7}Na_{0.3})Fe_{2-y}Se_2$ crystal at zero field. The upper inset shows the temperature range near the superconducting transition. The lower inset presents the real and the imaginary parts of the magnetic AC susceptibility.

of the sample preparation operations in the open air. During the preparation and mounting procedures for SEM and STM measurements the crystals were exposed to an open air for approximately 10–15 min.

First, the surface morphology of the sample was investigated in SEM (Carl Zeiss, Supra 40). At a characteristic scale of 1–20 μm, SEM images show an orthogonal stripes net structure as shown on Fig. 2. Similar structures with different proportions of dark and light areas have been repeatedly observed for intercalated iron selenides.[25] For our samples, the (planar) ratio of dark to light area is approximately 4:1. In our opinion, the observed contrast is simply due to different conductivity of phases. Another possible reason for a contrast could be a difference in a local chemical composition of phases. In Ref. [16], it was assumed that the different phases have different density and hardness, and therefore, the cleavage profile is formed by puncturing one phase from another. This idea contradicts the picture shown on the inset of Fig. 2. The inset shows the part of the sample with the intersection of a terrace with a light area. There is not any
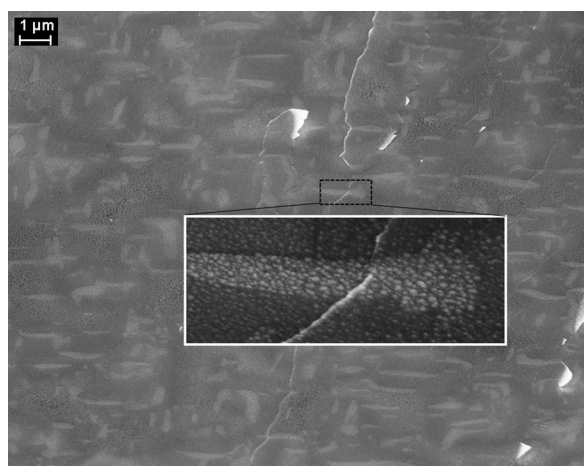

FIG. 2. Scanning Electron Microscopy image of the sample. Stripes net structure (bright regions) occupied ~25% of the area. The inset (image size 1,7, × 0,68 μm) shows closer view of the bright strip, which crosses a natural terrace on the sample surface.

noticeable distortion of the terrace edge at the light area border. This demonstrates that the mechanical properties of the dark and light parts are almost identical.

SEM images show lots of nanoscale structures of 10–20 nm on the surface of the sample. Since the sample was cleaved in an open air environment, it is likely that these particles appear due to a degradation process. It is interesting that degradation process lead to a uniform and dense formation of nanoparticles throughout the sample surface. For our mind it reflects a high order of the sample inhomogeneity on a nanoscale level which can serve as a seed for a new phase. These nanoparticles show slow "melting" (shape change) under electron beam exposure. Their sizes are reduced from scan to scan. This can be explained by the local sample heating. We did not observe these particles in ultra-high vacuum STM. The possible reason is a heat treatment of the sample in a ultra-high vacuum (UHV) chamber at 100–150 °C for about 2 h before scanning.

In general, the sample itself is not stable with respect to the electron beam scanning even at low accelerating (1–5 kV) voltages. Long time exposure caused the formation of dark spots, similar to the charged areas in non-conductive samples. Such behavior in investigated samples can be explained by a high mobility of the Na and K.

Topography and current-voltage characteristics (CVC) measurements were performed in an ultra-high vacuum STM system equipped with facilities for sample heating (JEOL JSTM-4500XT). The base pressure of the system is $\sim 1 \times 10^{-7}$ Pa. The STM tips were made from a tungsten wire by means of electrochemical etching in a 2N NaOH solution followed by baking in UHV.

STM images were taken in the constant current topographic (CCT) mode with the sample biased. CVC were made in Current Imaging Tunneling Spectroscopy (CITS) mode. Such measurement obtains a topographic image with the size of 128×128 points, and at the same time, carries out the CVC measurement at each image point.

As discussed above, we did not register any nanoparticles of the parasitic phase in the STM scans. We made the measurements of current-voltage characteristics together with topography measurements. Atomic resolution at room temperature was not achieved. The size of the scanned area ranged from 20×20 to 300×300 nm with the following parameters: tunnel voltage ± 0.2–3.5 V, tunnel current 20–1000 pA, and scanning velocity 0.1–1 Hz. The range of sweep voltage for CITS varied from $-0.3 \ldots +0.3$ V to $-3.5 \ldots +3.5$ V depending on STM tip tunneling conditions. We measured several CITS for the same area at different speeds of voltage sweep to avoid artifacts.

Our study revealed the existence of continuous regions with the essentially different types of current-voltage characteristics. In some regions, the current-voltage characteristics were noticeably more nonlinear than in others. For our mind it can correspond to a semiconducting and metallic phase distribution over the scanning area. Fig. 3 shows two typical current-voltage characteristics measured in -1–$+1$ V bias range and with the tip position defined by setting a tunnel current equal to 300 pA at 0.3 V bias. While both curves are non-liner one is also asymmetric and with larger amplitude.

(a)

(c)

(b)

(d)

FIG. 4. STM topography (a), the error of simulations with the Simmons formula (b), work function determined by the simulation (c), the module of the gradient of the averaged conductivity in the bias range −1–+1 V (d). Scan size—300 × 300 nm, Z scale 15 nm (a) and a.u. (b)–(d), a and b marks in 4(b) indicate the positions where CVC presented in Fig. 3 were recorded.
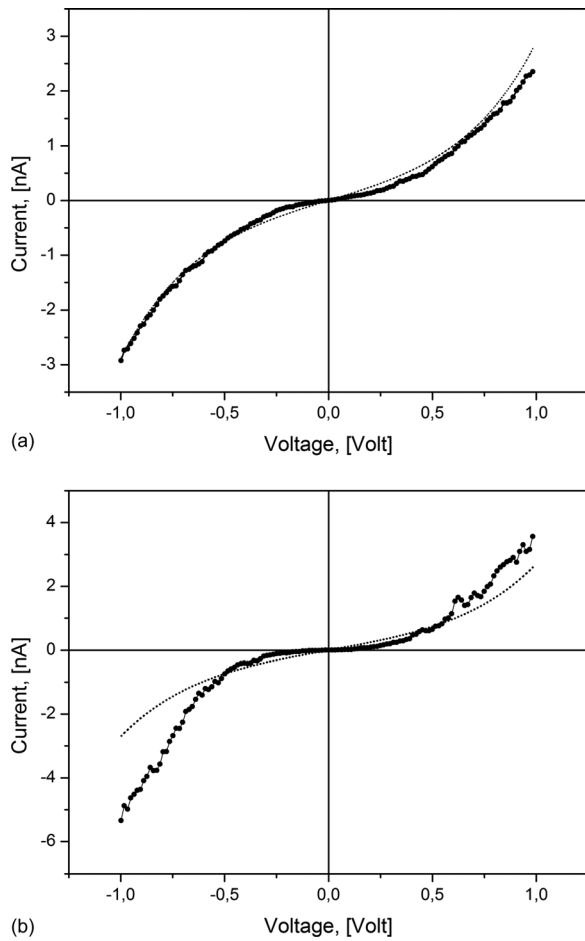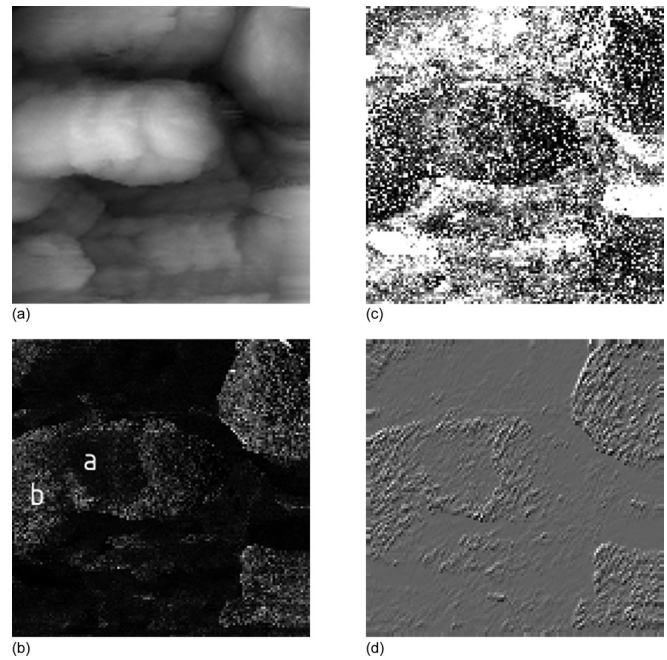

FIG. 3. CVC recorded at a metal (a) and semiconducting (b) regions of the sample (large dots) and CVC simulated for a metal-dielectric-metal structure (small dots). Exact positions are indicated by a and b marks in Fig. 4(b).

There are different sources for current-voltage nonlinearity in CITS. First of all, a transmission coefficient is not linear since the height of a tunnel barrier depends on an applied bias. For the typical values of work functions the transmission coefficient changes roughly one order at 1 V bias. Therefore, the current-voltage dependences for the bias range from −1 to +1 V are not ohmic even for the metal-dielectric-metal case. In the case of semiconductors, the density of states information is superimposed. The current-voltage dependence is an asymmetric since with a negative sample voltage a current tunnels out of the valence band, whereas for a positive voltage a current tunnels into the conduction band.

To evaluate the difference in current-voltage curve shapes we fitted them with the Simmons formula[26]

$$I = \alpha/^* \{ \exp[-\beta^* d^* (\varphi - V/2)^{1/2}](\varphi - V/2)$$
$$- \exp[-\beta^* d^* (\varphi + V/2)^{1/2}](\varphi + V/2)\}, \quad (1)$$

where I—tunnel current through the structure, d—dielectric width, V—bias applied to structure, ϕ—difference of metals work functions, α, β—constants.

This expression is a solution for a 1D metal-dielectric-metal tunnel junction in a quasi classical approximation. Therefore, it describes well the current—voltage nonlinearity

originating from a barrier suppression in the case of metal-dielectric-metal junction.

The fitting results for one of the CITS scanned areas are presented in Fig. 4. Figure 4(a) shows the topography of this area measured in CCT mode. Each of 16384 (128 × 128) current-voltage curves measured in this area was fitted with the Simmons formula by varying values of a work function and a tip-surface distance. Figure 4(b) shows the map of the fit error. The dark regions correspond to a small fitting error and the lighter regions to a large error. The small error means the Simmons formula fits well with the local CVC as it is expected for a metal surface. The large error means the Simmons formula does not follow the local CVC as it is expected for a semiconducting surface. Figure 4(c) shows the work function obtained by the fitting procedure. This picture looks well correlated with Fig. 4(b). It is worth to note that the work function is the only parameter in the Simmons formula which determines a CVC curvature. Thus, the change in the work function may compensate for the local density contribution and Fig. 4(c) can be expected to be a negative of Fig. 4(b).

Figure 4(d) shows the map of the module of the gradient of a conductivity averaged over from −1 to +1 V bias range. It is seen that this gradient is near zero and hardly changes for the dark (metal) regions of Fig. 4(b), whereas it varies considerably over the semiconducting regions. This behavior emphasizes the fundamental difference between measured current-voltage curves in these regions. For the metal regions, the CVC are nearly same due to the fixed initial conditions. For the semiconducting regions CVC are vary significantly along with local densities of state.

STM probes the surface properties, which depends, in particular, on the local surface contamination and other

surface imperfections. In the case of manganites, the correlation between a CVC shape and a local conductivity can be directly confirmed by applying of an external magnetic field.[27] To confirm the origin of a CVC variation for our sample, it is necessary to trace the properties of regions down to the superconducting transition. Unfortunately, it can be hampered by the fast conductivity vanishing in semiconducting regions as the temperature decreases. Perhaps less obvious, another possible conformation of a phase separation could be a direct correlation of the SEM contrast and the STM local properties. Our scans usually showed parts of a few domains going beyond the scanned area. This indicates that the averaged domain size is bigger than the scanned area sizes. Therefore, the domain size can be estimated in order of hundreds of nanometers that is close to the transverse dimensions of the light stripes on the SEM images.

IV. CONCLUSIONS

We have investigated the microstructure of the iron selenide superconductor $(K_{0.7}Na_{0.3})Fe_{2-y}Se_2$ with $T_c = 32$ K and near 100% Meissner screening volume fraction. Our STM studies suggest that, at room temperature, the sample shows spatial variations of the local electronic properties. Fitting of the local current-voltage curves with the Simmons model for metal-dielectric-metal structure confirmed a phase separation in the sample to a metal and semiconducting phases. The average size of the phase regions lies in the range of several tenth of a micrometer that reflect the microscale character of the phase separation.

ACKNOWLEDGMENTS

[1]J. K. Hulm, J. E. Kunzler, and B. T. Matthias, Phys. Today **34**(1), 34 (1981).

[2]K. Gofryk, M. Pan, C. Cantoni, B. Saparov, J. E. Mitchell, and A. S. Sefat, Phys. Rev. Lett. **112**, 047005 (2014).

[3]W. Bao, Y. Qiu, Q. Huang, M. A. Green, P. Zajdel, M. R. Fitzsimmons, M. Zhernenkov, S. Chang, M. Fang, B. Qian, E. K. Vehstedt, J. Yang, H. M. Pham, L. Spinu, and Z. Q. Mao, Phys. Rev. Lett. **102**, 247001 (2009).

[4]M. J. Han and S. Y. Savrasov, Phys. Rev. Lett. **103**, 067001 (2009).

[5]Y. Mizuguchi, K. Hamada, K. Goto, H. Takatsu, H. Kadowaki, and O. Miura, Solid State Commun. **152**, 1047 (2012).

[6]N. Katayama, S. Ji, D. Louca, S. Lee, M. Fujita, T. J. Sato, J. Wen, Z. Xu, G. Gu, G. Xu, Z. Lin, M. Enoki, S. Chang, K. Yamada, and J. M. Tranquada, J. Phys. Soc. Jpn. **79**, 113702 (2010).

[7]S. C. Speller, T. B. Britton, G. Hughes, S. Lozano-Perez, A. T. Boothroyd, E. Pomjakushina, K. Conder, and C. R. M. Grovenor, Appl. Phys. Lett. **99**, 192504 (2011).

[8]Y. A. Ovchenkov, D. A. Chareev, E. S. Kozlyakova, O. S. Volkova, and A. N. Vasiliev, Physica C **489**, 32 (2013).

[9]J. Guo, S. Jin, G. Wang, S. Wang, K. Zhu, T. Zhou, M. He, and X. Chen, Phys. Rev. B **82**, 180520 (2010).

[10]I. R. Shein and A. L. Ivanovski, Phys. Lett. A **375**, 1028 (2011).

[11]M. Gurvitch, Phys. Rev. B **24**, 7404 (1981).

[12]J. T. Park, D. S. Inosov, C. Niedermayer, G. L. Sun, D. Haug, N. B. Christensen, R. Dinnebier, A. V. Boris, A. J. Drew, L. Schulz, T. Shapoval, U. Wolff, V. Neu, X. Yang, C. T. Lin, B. Keimer, and V. Hinkov, Phys. Rev. Lett. **102**, 117006 (2009).

[13]Z. Shermadini, A. Krzton-Maziopa, M. Bendele, R. Khasanov, H. Luetkens, K. Conder, E. Pomjakushina, S. Weyeneth, V. Pomjakushin, O. Bossen, and A. Amato, Phys. Rev. Lett. **106**, 117602 (2011).

[14]C. N. Wang, P. Marsik, R. Schuster, A. Dubroka, M. Rössle, C. Niedermayer, G. D. Varma, A. F. Wang, X. H. Chen, T. Wolf, and C. Bernhard, Phys. Rev. B **85**, 214503 (2012).

[15]D. P. Shoemaker, D. Y. Chung, H. Claus, M. C. Francisco, S. Avci, A. Llobet, and M. G. Kanatzidis, Phys. Rev. B **86**, 184511 (2012).

[16]A. Charnukha, A. Cvitkovic, T. Prokscha, D. Pröpper, N. Ocelic, A. Suter, Z. Salman, E. Morenzoni, J. Deisenhofer, V. Tsurkan, A. Loidl, B. Keimer, and A. V. Boris, Phys. Rev. Lett. **109**, 017003 (2012).

[17]B. Shen, B. Zeng, G. F. Chen, J. B. He, D. M. Wang, H. Yang, and H. H. Wen, EPL **96**, 37010 (2011).

[18]N. Garcia, S. Vieira, A. M. Baro, J. Tornero, L. Vazquez, J. Gomez, A. Aguilo, S. Bourgeal, A. Buendia, M. Hortal, M. A. Lopez de la Torre, M. A. Ramos, R. Villar, K. V. Rao, D. X. Chen, J. Nogues, and N. Karpe, J. Appl. Phys. **63**, 4213 (1988).

[19]W. Li, H. Ding, P. Deng, K. Chang, C. Song, K. He, L. Wang, X. Ma, J. P. Hu, X. Chen, and Q. K. Xue, Nat. Phys. **8**, 126 (2012).

[20]J. E. Hoffman, Rep. Prog. Phys. **74**, 124513 (2011).

[21]P. Cai, C. Ye, W. Ruan, X. D. Zhou, A. F. Wang, M. Zhang, X.-H. Chen, and Y.-Y. Wang, Phys. Rev. B **85**, 094512 (2012).

[22]M. Fath, S. Freisem, A. A. Menovsky, Y. Tomioka, J. Aarts, and J. A. Mydosh, Science **285**, 1540 (1999).

[23]M. V. Roslova, S. A. Kuzmichev, T. E. Kuzmicheva, Y. A. Ovchenkov, M. Liu, I. V. Morozov, A. I. Boltalin, A. V. Shevelkov, and A. N. Vasiliev, CrystEngComm **16**, 6919–6928 (2014).

[24]C.-H. Li, B. Shen, F. Han, X. Zhu, and H.-H. Wen, Phys. Rev. B **83**, 184521 (2011).

[25]Z. Wang, Y. Cai, H.-X. Yang, H.-F. Tian, Z.-W. Wang, C. Ma, Z. Chen, and J.-Q. Li, Chin. Phys. B **22**, 087409 (2013).

[26]J. G. Simmons, J. Appl. Phys. **35**, 2472 (1964); **34**(6), 1793 (1963).

[27]S. F. Chen, P. I. Lin, J. Y. Juang, T. M. Uen, K. H. Wu, Y. S. Gou, and J. Y. Lin, Appl. Phys. Lett. **82**, 1242 (2003).